7th EUROMECH Solid Mechanics Conference
J. Ambrósio et.al. (eds.)
Lisbon, Portugal, September 7-11, 2009

EFFECTIVE GEOMETRICALLY EXACT PIEZOELECTRIC SOLID-SHELL ELEMENT BASED ON 3D ANALYTICAL INTEGRATION

Gennady M. Kulikov and Svetlana V. Plotnikova

Tambov State Technical University
Sovetskaya Street, 106, Tambov 392000, Russia
{kulikov, plotnikova}@apmath.tstu.ru

Keywords: Piezoelectric Laminated Shell, Geometrically Exact Four-Node Solid-Shell Element, 7-Parameter Shell Model.

Abstract. *The present work focuses on the development of the geometrically exact piezoelectric four-node solid-shell element based on the first-order 7-parameter equivalent single-layer theory, which permits to utilize the 3D constitutive equations. The term "geometrically exact" reflects the fact that the reference surface geometry is described by analytically given functions, in particular spline functions, and displacement vectors are resolved in the reference surface frame. As fundamental shell unknowns, six displacements of the outer surfaces and a transverse displacement of the midsurface are chosen. Such choice of displacements gives the possibility to derive strain-displacement relationships, which are invariant under rigid-body shell motions in a convected curvilinear coordinate system. To avoid shear and membrane locking and have no spurious zero energy modes, the assumed strain and stress resultant fields are invoked. As a result the geometrically exact hybrid piezoelectric solid-shell element developed does not contain any spurious zero energy modes and its stiffness matrix possesses a correct rank. Moreover, the elemental matrices require only direct substitutions and they are evaluated by using the 3D analytical integration.*

1 INTRODUCTION

A large number of works has been carried out on the 3D continuum-based finite elements that can handle analyses of thin piezoelectric laminated composite shells satisfactorily. These elements are typically defined by two layers of nodes at the bottom and top surfaces of the shell with three displacement degrees of freedom per node and known as isoparametric piezoelectric solid-shell elements. In the isoparametric solid-shell element formulation, initial and deformed geometry are equally interpolated allowing one to describe rigid-body motions precisely. The development of piezoelectric solid-shell elements was not straightforward. In order to overcome element deficiencies such as shear, membrane and curvature thickness locking, the ANS hybrid stress [1], hybrid strain [2] and hybrid stress-strain [3] finite element formulations were applied. Still, the isoparametric piezoelectric solid-shell element formulation is computationally inefficient because stresses and strains are analyzed in the global and local orthogonal Cartesian coordinate systems, although the normalized element coordinates represent already convected curvilinear coordinates.

To a more efficient finite element formulation one can arrive utilizing the geometrically exact (GEX) piezoelectric solid-shell elements that finds its point of departure in papers [4, 5]. This GEX piezoelectric solid-shell element formulation is based on the strain-displacement relationships of the first-order 6-parameter equivalent single-layer (ESL) theory. It is worth noting that these strain-displacement relationships precisely represent all rigid-body shell motions in any convected curvilinear coordinate system and no assumptions except for Timoshenko-Mindlin kinematics are required to derive them [6, 7]. For this purpose, the displacement vectors of bottom and top surfaces of the shell are introduced but resolved, in contrast with the isoparametric solid-shell element formulation, in the reference surface frame.

It is well-known that the 6-parameter piezoelectric solid-shell formulation on the basis of the complete 3D constitutive equations is deficient because thickness locking occurs. This is due to the fact that the linear displacement field in the thickness direction results in a constant transverse normal strain, which in turn causes artificial stiffening of the shell element in the case of non-vanishing Poisson's ratios. In order to circumvent a locking phenomenon, the 3D constitutive equations have to be modified [2, 4]. However, the use of complete 3D constitutive laws within the piezoelectric shell analysis is of great importance for engineering applications [8]. Thus, the first-order 7-parameter ESL piezoelectric shell model is best suited for this purpose because such a model is optimal with respect to the number of degrees of freedom employed.

The proposed 7-parameter ESL piezoelectric shell model is based on introducing six displacements of the outer surfaces and a transverse displacement of the midsurface as fundamental shell unknowns. Such choice of displacements gives the possibility to represent the GEX solid-shell element formulation in a very compact form and to derive strain-displacement relationships, which are invariant again under rigid-body motions in convected curvilinear coordinates [9]. It is also assumed that the electric potential is linear through the thickness of the piezoelectric layer and all displacement and electric potential degrees of freedom are coupled via constitutive equations. This allows us to formulate the efficient four-node *curved* solid-shell element for the analysis of thin piezoelectric laminated shells. To avoid shear and membrane locking and have no spurious zero energy modes, the assumed strain and stress resultant fields are invoked. This approach was developed for the 6- and 7-parameter GEX solid-shell element formulations in [4, 6, 9]. Herein, this hybrid stress-strain formulation is extended to the GEX piezoelectric four-node solid-shell element based on the 7-parameter ESL shell theory.

Taking into account that displacement vectors of outer and middle surfaces of the shell are resolved in the reference surface frame, the proposed GEX piezoelectric solid-shell element formulation has computational advantages compared to the conventional isoparametric solid-shell element formulations, since it reduces the computational cost of numerical integration in the evaluation of the stiffness matrix. This is due to the fact that, first, the element matrix developed requires only direct substitutions, i.e., no numerical matrix inversion is needed. The latter is unusual for the isoparametric hybrid/mixed shell element formulations. Second, we use the efficient 3D analytical integration [10] that permits to employ coarse meshes. Therefore, the GEX four-node solid-shell element developed is promising because of the fact that electric signals generated by sensors are fed into microprocessors, which in turn must activate a system of piezoelectric actuators in *real time*.

2 STRAIN-DISPLACEMENT RELATIONSHIPS

Consider a shell built up in the general case by the arbitrary superposition across the wall thickness of N thin layers of the uniform thickness $h_n = z_n - z_{n-1}$ including the ℓth piezoelectric layer (PZT) as shown in Figure 1. The nth layer may be defined as a 3D body of volume V_n bounded by two surfaces Ω_{n-1} and Ω_n, located at the distances $|z_{n-1}|$ and $|z_n|$ measured with respect to the reference surface Ω, and the edge boundary surface Σ_n. It is assumed that the bounding surfaces Ω_{n-1} and Ω_n are continuous, sufficiently smooth and without any singularities. Let the reference surface Ω be referred to the orthogonal curvilinear coordinates θ_1 and θ_2, which are referred to the lines of principal curvatures of its surface, whereas the coordinate θ_3 is oriented along the unit vector $\mathbf{e}_3$ normal to the reference surface; $\mathbf{e}_1$ and $\mathbf{e}_2$ are the unit vectors tangent to the lines of principal curvatures. Here and in the following developments, the index n identifies the belonging of any quantity to the nth layer and runs from 1 to N; the index of the piezoelectric layer $\ell = i_1, i_2, \ldots, i_L$, where L is the number of piezoelectric layers bonded to the outer surfaces of the host structure or embedded into its body; Greek indices α, β range from 1 to 2; indices i, j range from 1 to 3; the superscript A identifies the belonging of any quantity to the bottom and top surfaces Ω^- and Ω^+, and takes values $-$ and $+$.

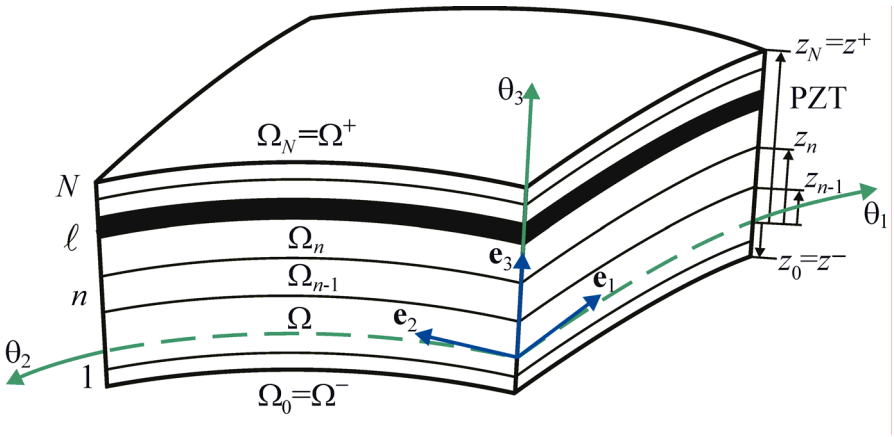

Figure 1: Laminated shell with embedded piezoelectric layer (PZT).

The displacement field is approximated in the thickness direction according to [11]:

$$u_\alpha = N^- u_\alpha^- + N^+ u_\alpha^+, \qquad u_3 = L^- u_3^- + L^{\mathrm{M}} u_3^{\mathrm{M}} + L^+ u_3^+ \tag{1}$$

$$N^- = \frac{1}{h}\left(z^+ - \theta_3\right), \qquad N^+ = \frac{1}{h}\left(\theta_3 - z^-\right) \tag{2}$$

$$L^- = N^-\left(N^- - N^+\right), \qquad L^{\mathrm{M}} = 4N^- N^+, \qquad L^+ = N^+\left(N^+ - N^-\right) \tag{3}$$

where $N^A(\theta_3)$ and $L^A(\theta_3)$, $L^{\mathrm{M}}(\theta_3)$ are the Lagrange polynomials of the first and second orders, respectively; $h = z^+ - z^-$ is the thickness of the shell; $z^- = z_0$ and $z^+ = z_N$ are the transverse coordinates of bottom and top surfaces of the shell; $u_i^A(\theta_1,\theta_2)$ are the components of the displacement vectors of the bottom and top surfaces, which are represented in the reference surface frame as follows:

$$\mathbf{u}^A = \sum_i u_i^A \mathbf{e}_i \tag{4}$$

and $u_3^{\mathrm{M}}(\theta_1,\theta_2)$ is the transverse displacement of the midsurface Ω^{M}.

The strain-displacement relationships of the first-order 7-parameter shell model [9] can be written as

$$\begin{gathered}\varepsilon_{\alpha\beta} = N^-\varepsilon_{\alpha\beta}^- + N^+\varepsilon_{\alpha\beta}^+, \qquad \varepsilon_{33} = N^-\varepsilon_{33}^- + N^+\varepsilon_{33}^+ \\ \varepsilon_{\alpha 3} = \varepsilon_{\alpha 3}^{\mathrm{M}}, \qquad \varepsilon_{\alpha 3}^{\mathrm{M}} = \frac{1}{2}\left(\varepsilon_{\alpha 3}^- + \varepsilon_{\alpha 3}^+\right)\end{gathered} \tag{5}$$

Here, $\varepsilon_{ij}^A(\theta_1,\theta_2)$ are the components of the strain tensor of outer surfaces of the shell expressed as

$$\begin{gathered}2\varepsilon_{\alpha\beta}^A = c_\alpha^A \lambda_{\alpha\beta}^A + c_\beta^A \lambda_{\beta\alpha}^A, \qquad \varepsilon_{33}^A = \beta_3^A \\ 2\varepsilon_{\alpha 3}^A = c_\alpha^A \beta_\alpha^A + \lambda_{3\alpha}^A\end{gathered} \tag{6}$$

where

$$\begin{gathered}\lambda_{\alpha\alpha}^A = \left(\frac{1}{A_\alpha}u_\alpha^A\right)_{,\alpha} + B_{\alpha\alpha}u_\alpha^A + B_{\alpha\beta}u_\beta^A + k_\alpha u_3^A \qquad (\beta \neq \alpha) \\ \lambda_{\beta\alpha}^A = \left(\frac{1}{A_\alpha}u_\beta^A\right)_{,\alpha} + B_{\alpha\alpha}u_\beta^A - B_{\alpha\beta}u_\alpha^A \qquad (\beta \neq \alpha) \\ \lambda_{3\alpha}^A = \left(\frac{1}{A_\alpha}u_3^A\right)_{,\alpha} + B_{\alpha\alpha}u_3^A - k_\alpha u_\alpha^A \\ \beta_i^- = \frac{1}{h}\left(-3u_i^- + 4u_i^{\mathrm{M}} - u_i^+\right), \qquad \beta_i^+ = \frac{1}{h}\left(u_i^- - 4u_i^{\mathrm{M}} + 3u_i^+\right) \\ u_\alpha^{\mathrm{M}} = \frac{1}{2}\left(u_\alpha^- + u_\alpha^+\right), \qquad c_\alpha^A = 1 + k_\alpha z^A, \qquad B_{\alpha\beta} = \frac{1}{A_\alpha A_\beta}A_{\alpha,\beta}\end{gathered} \tag{7}$$

where A_α and k_α are the Lamé coefficients and principal curvatures of the reference surface; c_α^A are the components of the shifter tensor at outer surfaces of the shell; the abbreviation $(\,)_{,\alpha}$ implies the partial derivatives with respect to coordinates θ_α. It is noteworthy that strain-displacement relationships (5) and (6) are very attractive because they are invariant under all rigid-body shell motions [9]. Note also that derivatives from relations (7) have been written in a form that is best suited for applying high performance analytical integration schemes inside the element.

3 DESCRIPTION OF ELECTRIC FIELD

The electric potential inside the ℓth piezoelectric layer is also assumed to be linear in the thickness direction

$$\varphi_\ell = N_\ell^- \varphi_\ell^- + N_\ell^+ \varphi_\ell^+ \tag{8}$$

$$N_\ell^- = \frac{1}{h_\ell}(z_\ell - \theta_3), \qquad N_\ell^+ = \frac{1}{h_\ell}(\theta_3 - z_{\ell-1}) \tag{9}$$

where $\varphi_\ell^{\pm}(\theta_1,\theta_2)$ are the values of the electric potential on the bottom and top surfaces of the ℓth layer; $h_\ell = z_\ell - z_{\ell-1}$ is the thickness of the piezoelectric layer.

The relation between the electric field $\mathbf{E}^{(\ell)}$ and the electric potential φ_ℓ is given by

$$\mathbf{E}^{(\ell)} = -\nabla\varphi_\ell \tag{10}$$

that is,

$$E_\alpha^{(\ell)} = -N_\ell^- \varphi_{\ell,\alpha}^- - N_\ell^+ \varphi_{\ell,\alpha}^+, \qquad E_3^{(\ell)} = -\frac{1}{h_\ell}\left(\varphi_\ell^+ - \varphi_\ell^-\right) \tag{11}$$

where $E_i^{(\ell)}$ are the components of the electric field of the ℓth layer. It is seen that the normal component of the electric field is constant through the thickness of the piezoelectric layer.

4 CONSTITUTIVE EQUATIONS

The constitutive equations of linear piezoelectricity [8, 12] for the monoclinic piezoelectric layer with reflectional symmetry in surfaces parallel to the reference surface can be expressed as

$$\boldsymbol{\varepsilon} = \mathbf{A}^{(\ell)}\boldsymbol{\sigma}^{(\ell)} + \left(\mathbf{d}^{(\ell)}\right)^{\mathrm{T}}\mathbf{E}^{(\ell)} \tag{12}$$

$$\mathbf{D}^{(\ell)} = \mathbf{d}^{(\ell)}\boldsymbol{\sigma}^{(\ell)} + \boldsymbol{\varsigma}^{(\ell)}\mathbf{E}^{(\ell)} \tag{13}$$

where $\boldsymbol{\varepsilon}$ is the strain vector; $\boldsymbol{\sigma}^{(\ell)}$ is the stress vector; $\mathbf{E}^{(\ell)}$ is the electric field vector; $\mathbf{D}^{(\ell)}$ is the electric displacement vector; $\mathbf{A}^{(\ell)}$ is the elastic compliance matrix; $\mathbf{d}^{(\ell)}$ is the piezoelectric matrix; $\boldsymbol{\varsigma}^{(\ell)}$ is the dielectric matrix defined by

$$\begin{gathered}\boldsymbol{\varepsilon} = \left[\varepsilon_{11}\ \varepsilon_{22}\ \varepsilon_{33}\ 2\varepsilon_{23}\ 2\varepsilon_{13}\ 2\varepsilon_{12}\right]^{\mathrm{T}}, \quad \boldsymbol{\sigma}^{(\ell)} = \left[\sigma_{11}^{(\ell)}\ \sigma_{22}^{(\ell)}\ \sigma_{33}^{(\ell)}\ \sigma_{23}^{(\ell)}\ \sigma_{13}^{(\ell)}\ \sigma_{12}^{(\ell)}\right]^{\mathrm{T}} \\ \mathbf{E}^{(\ell)} = \left[E_1^{(\ell)}\ E_2^{(\ell)}\ E_3^{(\ell)}\right]^{\mathrm{T}}, \quad \mathbf{D}^{(\ell)} = \left[D_1^{(\ell)}\ D_2^{(\ell)}\ D_3^{(\ell)}\right]^{\mathrm{T}}\end{gathered} \tag{14}$$

$$\mathbf{A}^{(\ell)}=\begin{bmatrix} A_{11}^{(\ell)} & A_{12}^{(\ell)} & A_{13}^{(\ell)} & 0 & 0 & A_{16}^{(\ell)} \\ & A_{22}^{(\ell)} & A_{23}^{(\ell)} & 0 & 0 & A_{26}^{(\ell)} \\ & & A_{33}^{(\ell)} & 0 & 0 & A_{36}^{(\ell)} \\ & & & A_{44}^{(\ell)} & A_{45}^{(\ell)} & 0 \\ & & & & A_{55}^{(\ell)} & 0 \\ \text{sym.} & & & & & A_{66}^{(\ell)} \end{bmatrix} \tag{15}$$

$$\mathbf{d}^{(\ell)}=\begin{bmatrix} 0 & 0 & 0 & d_{14}^{(\ell)} & d_{15}^{(\ell)} & 0 \\ 0 & 0 & 0 & d_{24}^{(\ell)} & d_{25}^{(\ell)} & 0 \\ d_{31}^{(\ell)} & d_{32}^{(\ell)} & d_{33}^{(\ell)} & 0 & 0 & d_{36}^{(\ell)} \end{bmatrix}, \quad \boldsymbol{\varsigma}^{(\ell)}=\begin{bmatrix} \varsigma_{11}^{(\ell)} & \varsigma_{12}^{(\ell)} & 0 \\ & \varsigma_{22}^{(\ell)} & 0 \\ \text{sym.} & & \varsigma_{33}^{(\ell)} \end{bmatrix}$$

Solving constitutive equations (12) for stresses and substituting stresses in constitutive equations (13), one obtains

$$\boldsymbol{\sigma}^{(\ell)}=\mathbf{C}^{(\ell)}\boldsymbol{\varepsilon}-\left(\mathbf{e}^{(\ell)}\right)^{\mathrm{T}}\mathbf{E}^{(\ell)} \tag{16}$$

$$\mathbf{D}^{(\ell)}=\mathbf{e}^{(\ell)}\boldsymbol{\varepsilon}+\in^{(\ell)}\mathbf{E}^{(\ell)} \tag{17}$$

where $\mathbf{C}^{(\ell)}$ is the material stiffness matrix; $\mathbf{e}^{(\ell)}$ and $\in^{(\ell)}$ are the piezoelectric and dielectric matrices expressed as

$$\mathbf{C}^{(\ell)}=\left(\mathbf{A}^{(\ell)}\right)^{-1}, \qquad \mathbf{e}^{(\ell)}=\mathbf{d}^{(\ell)}\mathbf{C}^{(\ell)}, \qquad \in^{(\ell)}=\boldsymbol{\varsigma}^{(\ell)}-\mathbf{d}^{(\ell)}\mathbf{C}^{(\ell)}\left(\mathbf{d}^{(\ell)}\right)^{\mathrm{T}} \tag{18}$$

5 HU-WASHIZU VARIATIONAL EQUATION

The first-order 7-parameter piezoelectric ESL shell theory developed is based on the assumed approximations of displacements (1), displacement-dependent strains (5) and electric potential (8) in the thickness direction. Additionally, we accept the through-thickness approximation for the independently assumed strains as follows:

$$\hat{\varepsilon}_{\alpha\beta}=N^{-}\hat{\varepsilon}_{\alpha\beta}^{-}+N^{+}\hat{\varepsilon}_{\alpha\beta}^{+}, \qquad \hat{\varepsilon}_{33}=N^{-}\hat{\varepsilon}_{33}^{-}+N^{+}\hat{\varepsilon}_{33}^{+}, \qquad \hat{\varepsilon}_{\alpha 3}=\hat{\varepsilon}_{\alpha 3}^{\mathrm{M}} \tag{19}$$

where $\hat{\varepsilon}_{\alpha\beta}^{A}(\theta_1,\theta_2)$ and $\hat{\varepsilon}_{33}^{A}(\theta_1,\theta_2)$ are the assumed tangential and transverse normal strains of the bottom and top surfaces; $\hat{\varepsilon}_{\alpha 3}^{\mathrm{M}}(\theta_1,\theta_2)$ are the assumed transverse shear strains of the midsurface.

Substituting approximations (1), (5), (8) and (19) into the 3D Hu-Washizu functional [4] and allowing for that metrics of all surfaces parallel to the reference surface are identical and equal to the metric of the midsurface, one arrives at the 2D Hu-Washizu functional for the 7-parameter shell element

$$\begin{aligned} \mathit{\Pi}_{\mathrm{HW}}^{\mathrm{el}}=\int_{-1}^{1}\int_{-1}^{1}\Big[&\frac{1}{2}\hat{\boldsymbol{E}}^{\mathrm{T}}\mathbf{D}_{\mathrm{M}}\hat{\boldsymbol{E}}+\hat{\boldsymbol{E}}^{\mathrm{T}}\mathbf{D}_{\mathrm{ME}}^{(\ell)}\boldsymbol{\Psi}_{\ell}+\frac{1}{2}\boldsymbol{\Psi}_{\ell}^{\mathrm{T}}\mathbf{D}_{\mathrm{E}}^{(\ell)}\boldsymbol{\Psi}_{\ell} \\ &-\mathbf{H}^{\mathrm{T}}\left(\hat{\boldsymbol{E}}-\boldsymbol{E}\right)-\mathbf{v}^{\mathrm{T}}\mathbf{p}-\boldsymbol{\chi}_{\ell}^{\mathrm{T}}\mathbf{q}_{\ell}\Big]A_1^{\mathrm{el}}A_2^{\mathrm{el}}c_1^{\mathrm{M}}c_2^{\mathrm{M}}\mathrm{d}\xi_1\mathrm{d}\xi_2 \end{aligned} \tag{20}$$

Here, more convenient matrix notations are introduced

$$\begin{gathered}
\mathbf{v}=\left[u_1^- \; u_2^- \; u_3^- \; u_1^+ \; u_2^+ \; u_3^+ \; u_3^{\mathrm{M}}\right]^{\mathrm{T}}, \quad \boldsymbol{\chi}_\ell=\left[\varphi_\ell^- \; \varphi_\ell^+\right]^{\mathrm{T}}, \quad \boldsymbol{\Psi}_\ell=\left[\varphi_\ell^- \; \varphi_\ell^+ \; \varphi_{\ell,1}^- \; \varphi_{\ell,1}^+ \; \varphi_{\ell,2}^- \; \varphi_{\ell,2}^+\right]^{\mathrm{T}} \\
\boldsymbol{E}=\left[\varepsilon_{11}^- \; \varepsilon_{11}^+ \; \varepsilon_{22}^- \; \varepsilon_{22}^+ \; \varepsilon_{33}^- \; \varepsilon_{33}^+ \; 2\varepsilon_{12}^- \; 2\varepsilon_{12}^+ \; 2\varepsilon_{13}^{\mathrm{M}} \; 2\varepsilon_{23}^{\mathrm{M}}\right]^{\mathrm{T}} \\
\hat{\boldsymbol{E}}=\left[\hat{\varepsilon}_{11}^- \; \hat{\varepsilon}_{11}^+ \; \hat{\varepsilon}_{22}^- \; \hat{\varepsilon}_{22}^+ \; \hat{\varepsilon}_{33}^- \; \hat{\varepsilon}_{33}^+ \; 2\hat{\varepsilon}_{12}^- \; 2\hat{\varepsilon}_{12}^+ \; 2\hat{\varepsilon}_{13}^{\mathrm{M}} \; 2\hat{\varepsilon}_{23}^{\mathrm{M}}\right]^{\mathrm{T}} \\
\mathbf{H}=\left[H_{11}^- \; H_{11}^+ \; H_{22}^- \; H_{22}^+ \; H_{33}^- \; H_{33}^+ \; H_{12}^- \; H_{12}^+ \; H_{13} \; H_{23}\right]^{\mathrm{T}} \\
\mathbf{p}=\left[-p_1^- \; -p_2^+ \; -p_3^- \; p_1^+ \; p_2^+ \; p_3^+ \; 0\right]^{\mathrm{T}}, \quad \mathbf{q}_\ell=\left[q_\ell^- \; q_\ell^+\right]^{\mathrm{T}}
\end{gathered} \tag{21}$$

where $\mathbf{D}_{\mathrm{M}}$, $\mathbf{D}_{\mathrm{ME}}^{(\ell)}$ and $\mathbf{D}_{\mathrm{E}}^{(\ell)}$ are the mechanical, piezoelectric and dielectric constitutive matrices presented in Appendix A; $\xi_\alpha=\left(\theta_\alpha-d_\alpha^{\mathrm{el}}\right)/\ell_\alpha^{\mathrm{el}}$ are the normalized curvilinear elemental coordinates as shown in Figure 2; d_α^{el} are the coordinates of the center of the element; $2\ell_\alpha^{\mathrm{el}}$ are the lengths of the element in θ_α-directions; $A_\alpha^{\mathrm{el}}=A_\alpha\ell_\alpha^{\mathrm{el}}$ are the Lamé coefficients of the element reference surface; $c_\alpha^{\mathrm{M}}=1+k_\alpha\left(z^-+z^+\right)/2$ are the components of the shifter tensor at the midsurface; p_i^A are the tractions applied to the bottom and top surfaces; q_ℓ^A are the prescribed surface charge densities of the ℓth piezoelectric layer; $H_{\alpha\beta}^{\pm}$, $H_{33}^{\pm}$ and $H_{\alpha 3}$ are the stress resultants defined as

$$\begin{gathered}
H_{\alpha\beta}^A=\sum_n\int_{z_{n-1}}^{z_n}\sigma_{\alpha\beta}^{(n)}N^A\mathrm{d}\theta_3, \quad H_{33}^A=\sum_n\int_{z_{n-1}}^{z_n}\sigma_{33}^{(n)}N^A\mathrm{d}\theta_3 \\
H_{\alpha 3}=\sum_n\int_{z_{n-1}}^{z_n}\sigma_{\alpha 3}^{(n)}\mathrm{d}\theta_3
\end{gathered} \tag{22}$$

Remark 1. For the simplicity, we limit our discussion to the case of one piezoelectric layer, i.e., $L=1$ and $\ell=i_1\in\{1,\,2,\ldots,N\}$, since only a sign of the summation needs to be involved in equation (20) to generalize.

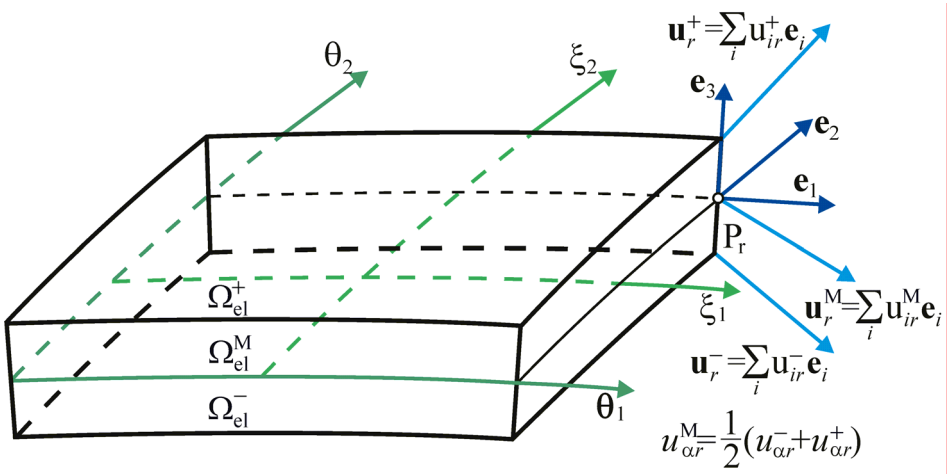

Figure 2: GEX piezoelectric solid-shell element based on the 7-parameter ESL shell model, where P_r is the element node (r=1, 2, …, NN).

Using the stationarity of the Hu-Washizu functional (20) with respect to the independent variables $\mathbf{v}$, $\hat{\boldsymbol{E}}$, $\mathbf{H}$ and $\boldsymbol{\chi}_\ell$, one can write the mixed variational equation as follows:

$$\delta \Pi_{\mathrm{HW}}^{\mathrm{el}} = 0 \tag{23}$$

6 FINITE ELEMENT FORMULATION

The finite element formulation is based on the simple and efficient approximation of shells via *curved four-node* piezoelectric solid-shell elements

$$\mathbf{v} = \sum_r N_r \mathbf{v}_r, \qquad \mathbf{v}_r = \left[u_{1r}^- \; u_{2r}^- \; u_{3r}^- \; u_{1r}^+ \; u_{2r}^+ \; u_{3r}^+ \; u_{3r}^{\mathrm{M}}\right]^{\mathrm{T}} \tag{24}$$

$$\boldsymbol{E} = \mathbf{B}_{\mathrm{M}}\mathbf{U}, \qquad \mathbf{U} = \left[\mathbf{v}_1^{\mathrm{T}} \; \mathbf{v}_2^{\mathrm{T}} \; \mathbf{v}_3^{\mathrm{T}} \; \mathbf{v}_4^{\mathrm{T}}\right]^{\mathrm{T}} \tag{25}$$

$$\boldsymbol{\chi}_\ell = \sum_r N_r \boldsymbol{\chi}_{\ell r}, \qquad \boldsymbol{\chi}_{\ell r} = \left[\varphi_{\ell r}^- \; \varphi_{\ell r}^+\right]^{\mathrm{T}} \tag{26}$$

$$\boldsymbol{\Psi}_\ell = \mathbf{B}_{\mathrm{E}}\boldsymbol{\Phi}_\ell, \qquad \boldsymbol{\Phi}_\ell = \left[\boldsymbol{\chi}_{\ell 1}^{\mathrm{T}} \; \boldsymbol{\chi}_{\ell 2}^{\mathrm{T}} \; \boldsymbol{\chi}_{\ell 3}^{\mathrm{T}} \; \boldsymbol{\chi}_{\ell 4}^{\mathrm{T}}\right]^{\mathrm{T}} \tag{27}$$

where $N_r(\xi_1, \xi_2)$ are the bilinear shape functions of the element; $\mathbf{v}_r$ and $\boldsymbol{\chi}_{\ell r}$ are the displacement and electric potential vectors of the element nodes; $\mathbf{B}_{\mathrm{M}}$ is the strain-displacement transformation matrix of order 10×28; $\mathbf{B}_{\mathrm{E}}$ is the piezoelectric transformation matrix of order 6×8; the index r runs from 1 to 4 and denotes the number of nodes.

To implement the analytical integration inside the element, it is convenient to rewrite interpolations (24)-(27) in the following form:

$$\mathbf{v} = \sum_{r_1, r_2} \xi_1^{r_1} \xi_2^{r_2} \mathbf{v}^{r_1 r_2} \tag{28}$$

$$\boldsymbol{E} = \sum_{r_1, r_2} \xi_1^{r_1} \xi_2^{r_2} \mathbf{B}_{\mathrm{M}}^{r_1 r_2} \mathbf{U} \tag{29}$$

$$\boldsymbol{\chi}_\ell = \sum_{r_1, r_2} \xi_1^{r_1} \xi_2^{r_2} \boldsymbol{\chi}_\ell^{r_1 r_2} \tag{30}$$

$$\boldsymbol{\Psi}_\ell = \sum_{r_1, r_2} \xi_1^{r_1} \xi_2^{r_2} \mathbf{B}_{\mathrm{E}}^{r_1 r_2} \boldsymbol{\Phi}_\ell \tag{31}$$

where $\mathbf{B}_{\mathrm{M}}^{r_1 r_2}$ and $\mathbf{B}_{\mathrm{E}}^{r_1 r_2}$ are the *constant* strain-displacement and piezoelectric transformation matrices throughout the element; the superscripts r_1, r_2 take the values 0 and 1.

Following a technique developed in [4, 9], we interpolate the assumed strains and stress resultants (21) inside the element as follows:

$$\hat{\boldsymbol{E}} = \sum_{r_1, r_2} \xi_1^{r_1} \xi_2^{r_2} \mathbf{Q}^{r_1 r_2} \hat{\boldsymbol{E}}^{r_1 r_2}$$

$$\hat{\boldsymbol{E}}^{00} = \left[\hat{\varepsilon}_{11}^{-00} \; \hat{\varepsilon}_{11}^{+00} \; \hat{\varepsilon}_{22}^{-00} \; \hat{\varepsilon}_{22}^{+00} \; \hat{\varepsilon}_{33}^{-00} \; \hat{\varepsilon}_{33}^{+00} \; 2\hat{\varepsilon}_{12}^{-00} \; 2\hat{\varepsilon}_{12}^{+00} \; 2\hat{\varepsilon}_{13}^{\mathrm{M}00} \; 2\hat{\varepsilon}_{23}^{\mathrm{M}00}\right]^{\mathrm{T}} \tag{32}$$

$$\hat{\boldsymbol{E}}^{01} = \left[\hat{\varepsilon}_{11}^{-01} \; \hat{\varepsilon}_{11}^{+01} \; \hat{\varepsilon}_{33}^{-01} \; \hat{\varepsilon}_{33}^{+01} \; 2\hat{\varepsilon}_{13}^{\mathrm{M}01}\right]^{\mathrm{T}}, \; \hat{\boldsymbol{E}}^{10} = \left[\hat{\varepsilon}_{22}^{-10} \; \hat{\varepsilon}_{22}^{+10} \; \hat{\varepsilon}_{33}^{-10} \; \hat{\varepsilon}_{33}^{+10} \; 2\hat{\varepsilon}_{23}^{\mathrm{M}10}\right]^{\mathrm{T}}, \; \hat{\boldsymbol{E}}^{11} = \left[\hat{\varepsilon}_{33}^{-11} \; \hat{\varepsilon}_{33}^{+11}\right]^{\mathrm{T}}$$

and

$$\mathbf{H} = \sum_{r_1,r_2} \xi_1^{r_1} \xi_2^{r_2} \mathbf{Q}^{r_1 r_2} \mathbf{H}^{r_1 r_2}$$

$$\mathbf{H}^{00} = \left[H_{11}^{-00}\ H_{11}^{+00}\ H_{22}^{-00}\ H_{22}^{+00}\ H_{33}^{-00}\ H_{33}^{+00}\ H_{12}^{-00}\ H_{12}^{+00}\ H_{13}^{00}\ H_{23}^{00}\right]^{\mathrm{T}} \tag{33}$$

$$\mathbf{H}^{01} = \left[H_{11}^{-01} H_{11}^{+01} H_{33}^{-01} H_{33}^{+01} H_{13}^{01}\right]^{\mathrm{T}}, \mathbf{H}^{10} = \left[H_{22}^{-10} H_{22}^{+10} H_{33}^{-10} H_{33}^{+10} H_{23}^{10}\right]^{\mathrm{T}}, \mathbf{H}^{11} = \left[H_{33}^{-11}\ H_{33}^{+11}\right]^{\mathrm{T}}$$

where $\mathbf{Q}^{00}$ is the identity matrix of order 10×10, whereas

$$\mathbf{Q}^{01} = \begin{bmatrix} 1&0&0&0&0\\ 0&1&0&0&0\\ 0&0&0&0&0\\ 0&0&0&0&0\\ 0&0&1&0&0\\ 0&0&0&1&0\\ 0&0&0&0&0\\ 0&0&0&0&0\\ 0&0&0&0&1\\ 0&0&0&0&0 \end{bmatrix}, \quad \mathbf{Q}^{10} = \begin{bmatrix} 0&0&0&0&0\\ 0&0&0&0&0\\ 1&0&0&0&0\\ 0&1&0&0&0\\ 0&0&1&0&0\\ 0&0&0&1&0\\ 0&0&0&0&0\\ 0&0&0&0&0\\ 0&0&0&0&0\\ 0&0&0&0&1 \end{bmatrix}, \quad \mathbf{Q}^{11} = \begin{bmatrix} 0&0\\ 0&0\\ 0&0\\ 0&0\\ 1&0\\ 0&1\\ 0&0\\ 0&0\\ 0&0\\ 0&0 \end{bmatrix}$$

Substituting interpolations (28)-(33) into the mixed variational equation (23) in conjunction with (20) and using a standard variational procedure, one obtains the element equilibrium equations

$$\begin{gathered} \hat{\boldsymbol{E}}^{r_1 r_2} = \left(\mathbf{Q}^{r_1 r_2}\right)^{\mathrm{T}} \mathbf{B}_{\mathrm{M}}^{r_1 r_2} \mathbf{U} \\ \mathbf{H}^{r_1 r_2} = \left(\mathbf{Q}^{r_1 r_2}\right)^{\mathrm{T}} \mathbf{D}_{\mathrm{M}} \mathbf{Q}^{r_1 r_2} \hat{\boldsymbol{E}}^{r_1 r_2} + \left(\mathbf{Q}^{r_1 r_2}\right)^{\mathrm{T}} \mathbf{D}_{\mathrm{ME}}^{(\ell)} \mathbf{B}_{\mathrm{E}}^{r_1 r_2} \boldsymbol{\Phi}_{\ell} \\ \sum_{r_1,r_2} \frac{1}{3^{r_1+r_2}} \left(\mathbf{B}_{\mathrm{M}}^{r_1 r_2}\right)^{\mathrm{T}} \mathbf{Q}^{r_1 r_2} \mathbf{H}^{r_1 r_2} = \mathbf{F}_{\mathrm{p}} \\ \sum_{r_1,r_2} \frac{1}{3^{r_1+r_2}} \left(\mathbf{B}_{\mathrm{E}}^{r_1 r_2}\right)^{\mathrm{T}} \left[\left(\mathbf{D}_{\mathrm{ME}}^{(\ell)}\right)^{\mathrm{T}} \mathbf{Q}^{r_1 r_2} \hat{\boldsymbol{E}}^{r_1 r_2} + \mathbf{D}_{\mathrm{E}}^{(\ell)} \mathbf{B}_{\mathrm{E}}^{r_1 r_2} \boldsymbol{\Phi}_{\ell} \right] = \mathbf{F}_{\mathrm{q}}^{(\ell)} \end{gathered} \tag{34}$$

where $\mathbf{F}_{\mathrm{p}}$ is the element-wise surface traction vector; $\mathbf{F}_{\mathrm{q}}^{(\ell)}$ is the element-wise electric force vector of the ℓth piezoelectric layer.

Eliminating further assumed strains and stress resultants from equilibrium equations (34), we obtain governing equations of the piezoelectric finite element

$$\begin{bmatrix} \mathbf{K}_{\mathrm{M}} & \mathbf{K}_{\mathrm{ME}}^{(\ell)} \\ \left(\mathbf{K}_{\mathrm{ME}}^{(\ell)}\right)^{\mathrm{T}} & \mathbf{K}_{\mathrm{E}}^{(\ell)} \end{bmatrix} \begin{bmatrix} \mathbf{U} \\ \boldsymbol{\Phi}_{\ell} \end{bmatrix} = \begin{bmatrix} \mathbf{F}_{\mathrm{p}} \\ \mathbf{F}_{\mathrm{q}}^{(\ell)} \end{bmatrix} \tag{35}$$

where $\mathbf{K}_{\mathrm{M}}$ is the stiffness matrix; $\mathbf{K}_{\mathrm{ME}}^{(\ell)}$ is the piezoelectric stiffness matrix; $\mathbf{K}_{\mathrm{E}}^{(\ell)}$ is the dielectric stiffness matrix defined as

$$\mathbf{K}_{\mathrm{M}} = \sum_{r_1,r_2} \frac{1}{3^{r_1+r_2}} \left(\mathbf{B}_{\mathrm{M}}^{r_1 r_2}\right)^{\mathrm{T}} \mathbf{Q}^{r_1 r_2} \left(\mathbf{Q}^{r_1 r_2}\right)^{\mathrm{T}} \mathbf{D}_{\mathrm{M}} \mathbf{Q}^{r_1 r_2} \left(\mathbf{Q}^{r_1 r_2}\right)^{\mathrm{T}} \mathbf{B}_{\mathrm{M}}^{r_1 r_2} \tag{36}$$

$$\mathbf{K}_{\mathrm{ME}}^{(\ell)} = \sum_{r_1,r_2} \frac{1}{3^{r_1+r_2}} \left(\mathbf{B}_{\mathrm{M}}^{r_1 r_2}\right)^{\mathrm{T}} \mathbf{Q}^{r_1 r_2} \left(\mathbf{Q}^{r_1 r_2}\right)^{\mathrm{T}} \mathbf{D}_{\mathrm{ME}}^{(\ell)} \mathbf{B}_{\mathrm{E}}^{r_1 r_2} \tag{37}$$

$$\mathbf{K}_{\mathrm{E}}^{(\ell)} = \sum_{r_1,r_2} \frac{1}{3^{r_1+r_2}} \left(\mathbf{B}_{\mathrm{E}}^{r_1 r_2}\right)^{\mathrm{T}} \mathbf{D}_{\mathrm{E}}^{(\ell)} \mathbf{B}_{\mathrm{E}}^{r_1 r_2} \tag{38}$$

Remark 2. The element stiffness matrix $\mathbf{K}_{\mathrm{M}}$ possesses six zero eigenvalues as required for satisfaction of the general rigid-body motion representation. This is due to the fact that 22 assumed strain parameters are accepted according to the approximation (32), whereas the GEX solid-shell element has seven displacement degrees of freedom per node exactly.

Remark 3. It is worth noting that all matrices (36)-(38) require only direct substitutions, that is, no inversion is needed for the GEX piezoelectric hybrid finite element formulation developed. This is unusual for the isoparametric hybrid/mixed shell element formulations.

Remark 4. The element matrices (36)-(38) are evaluated by using the analytical integration. A short discussion on that is presented in Appendix B. Therefore, the proposed GEX piezoelectric solid-shell element formulation is very economical and efficient compared to the conventional isoparametric piezoelectric finite element formulations because this improvement allows one to reduce the computational cost of numerical integration in the evaluation of the elemental matrices [4, 9].

For the actuator-embedded shell analysis when only a prescribed input voltage is applied, the governing finite element equations (35) are simplified and expressed as

$$\mathbf{K}_{\mathrm{M}}\mathbf{U} = -\mathbf{K}_{\mathrm{ME}}^{(\ell)}\mathbf{\Phi}_{\ell} \tag{39}$$

These equations have to be solved to assess a response of the coupled electromechanical system.

7 NUMERICAL EXAMPLES

The performance of the proposed GEX piezoelectric solid-shell element is evaluated with several problems extracted from the literature. The results are compared with those obtained by using robust isoparametric and GEX piezoelectric solid-shell elements. A listing of these elements and the abbreviations used to identify them are contained in Table 1.

Name	Description
GEX7P4	Geometrically exact hybrid stress-strain piezoelectric four-node solid-shell element developed on the basis of the 7-parameter model
GEX6P4	Geometrically exact hybrid stress-strain piezoelectric four-node solid-shell element based on the 6-parameter model [4]
ISO6P4	Isoparametric hybrid stress piezoelectric four-node solid-shell element based on the 6-parameter model [1, 13]
ISO6P9	Isoparametric hybrid strain piezoelectric nine-node solid-shell element based on the 6-parameter model [2]

Table 1: Listing of piezoelectric solid-shell elements.

7.1 Bimorph cantilever beam

We consider first a bimorph pointer [8] consisting of two identical PVDF layers, which have been polarized in opposite directions parallel to the thickness direction to induce internal

bending moments. The geometrical and material properties of the cantilever beam are shown in Figure 3. The electrical loading case is assumed to be a unit voltage applied across the beam thickness.

Table 2 displays the distribution of the transverse displacement along the beam axis using the 10×1 mesh of GEX7P4 elements and a comparison with exact and numerical solutions [2, 4, 8, 13]. One can observe that all finite element formulations perform well.

	Dimensionless coordinate θ_1 / a				
	0.2	0.4	0.6	0.8	1
Exact solution [8]	0.138	0.552	1.242	2.208	3.450
ISO6P4 [13]	0.138	0.552	1.242	2.208	3.450
ISO6P9 [2]	0.137	0.551	1.241	2.207	3.449
GEX6P4 [4]	0.138	0.552	1.242	2.208	3.450
GEX7P4	0.138	0.552	1.242	2.208	3.450

Table 2: Transverse midline displacement $u_3^{\mathrm{M}}\left(10^{-7}\,\mathrm{m}\right)$ of the bimorph cantilever beam.

7.2 Cantilever plate with segmented PZT actuators

Consider cylindrical bending of the homogeneous graphite/epoxy cantilever plate with segmented PZT-5A actuators attached to its bottom and top surfaces [14] as shown in Figure 4. The non-vanishing material parameters for graphite/epoxy are $c_{11} = 183.443\,\mathrm{GPa}$, $c_{22} = c_{33} = 11.662\,\mathrm{GPa}$, $c_{12} = c_{13} = 4.363\,\mathrm{GPa}$, $c_{23} = 3.918\,\mathrm{GPa}$, $c_{44} = 2.870\,\mathrm{GPa}$, $c_{55} = c_{66} = 7.170\,\mathrm{GPa}$; for PZT-5A are $c_{11} = c_{22} = 99.201\,\mathrm{GPa}$, $c_{33} = 86.856\,\mathrm{GPa}$, $c_{12} = 54.016\,\mathrm{GPa}$, $c_{13} = c_{23} = 50.778\,\mathrm{GPa}$, $c_{44} = c_{55} = 21.100\,\mathrm{GPa}$, $c_{66} = 22.593\,\mathrm{GPa}$, $e_{31} = e_{32} = -7.209\,\mathrm{C/m^2}$, $e_{33} = 15.118\ \mathrm{C/m^2}$, $e_{24} = e_{15} = 12.322\ \mathrm{C/m^2}$. The actuators are polarized in opposite directions parallel to the θ_3-direction and subjected, first, to the same constant voltage $\hat{\varphi}$ to induce the extensional actuation. Then, applying opposite electric potentials $-\hat{\varphi}$ and $\hat{\varphi}$ to the outer patches surfaces, we induce the bending actuation. The electrodes on the interfaces are assumed to be at the zero potential.

Figure 5 presents the longitudinal distribution of non-dimensional midplane displacements $\overline{u}_i = u_i^{\mathrm{M}} c_0 / e_{31}\hat{\varphi}$, where $c_0 = 99.201\,\mathrm{GPa}$ for both actuation problems, by using 16 GEX7P4 elements. A comparison with exact and finite element solutions [5, 14] is also represented. As can be seen, the 6-parameter shell model overestimates the tip displacement by 13 % in the extensional actuation and by 10 % in the bending one.

7.3 Simply supported plate with PZT actuators

This example demonstrates the shape control of the laminated composite plate through bending actuation. A simply supported plate with PZT G1195 actuators bonded to the outer surfaces is initially subjected to uniform pressure of 200 Pa [15]. The plate core is composed of six graphite/epoxy layers with stacking sequence $[0/90/0]_{\mathrm{S}}$. The geometrical data of the problem are presented in Figure 6. The non-vanishing material parameters for graphite/epoxy are $E_{11} = 150\,\mathrm{GPa}$, $E_{22} = E_{33} = 9\,\mathrm{GPa}$, $\nu_{12} = \nu_{13} = 0.3$, $\nu_{23} = 0.49$, $G_{12} = G_{13} = 7.1\,\mathrm{GPa}$, $G_{23} = 3\,\mathrm{GPa}$; for PZT G1195 are $E = 63\,\mathrm{GPa}$, $\nu = 0.3$, $G = 24.2\,\mathrm{GPa}$, $d_{31} = d_{32} = 254\,\mathrm{pm/V}$.

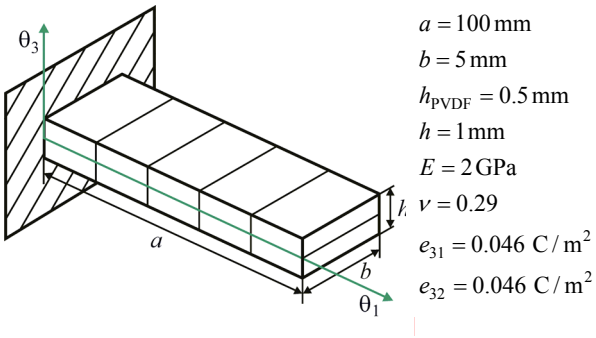

Figure 3: Cantilever bimorph beam.

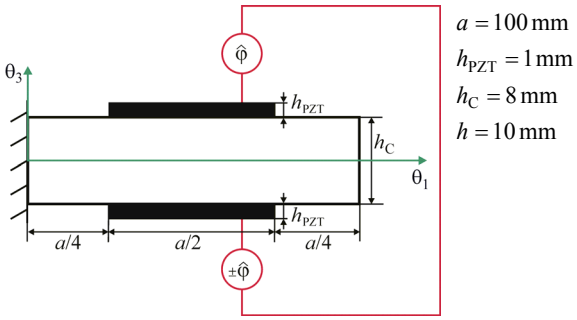

Figure 4: Cantilever plate with segmented PZT actuators.

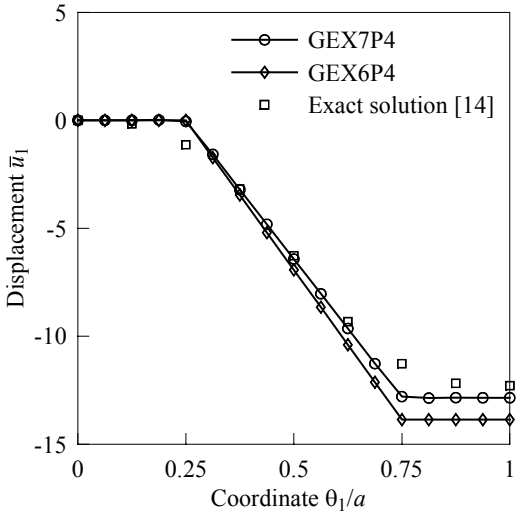

(a)

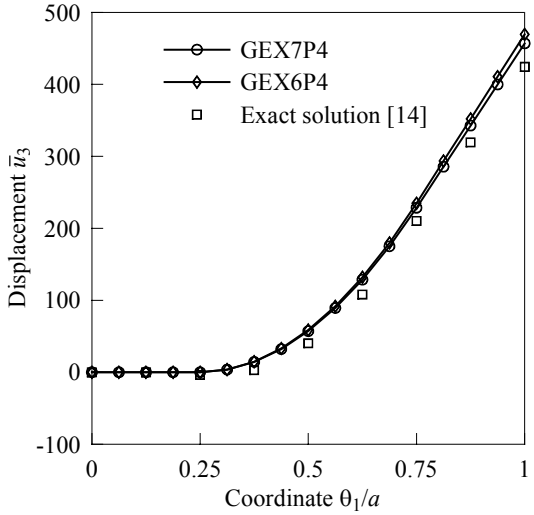

(b)

Figure 5: Midplane displacements of the cantilever plate with segmented PZT actuators: (a) axial displacement $\bar{u}_1$ in extensional actuation and (b) transverse displacement $\bar{u}_3$ in bending actuation.

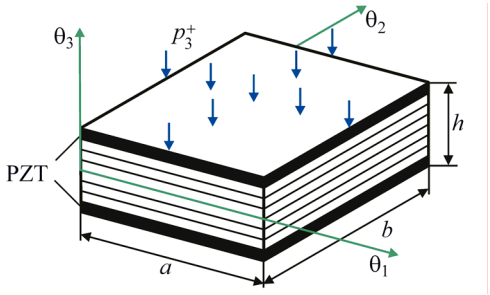

$a = b = 0.254$ m, $h_{PZT} = 0.254$ mm, $h_C = 0.828$ mm
$h = 1.336$ mm, $p_3^+ = -200$ Pa

Figure 6: Simply supported plate with PZT actuators.

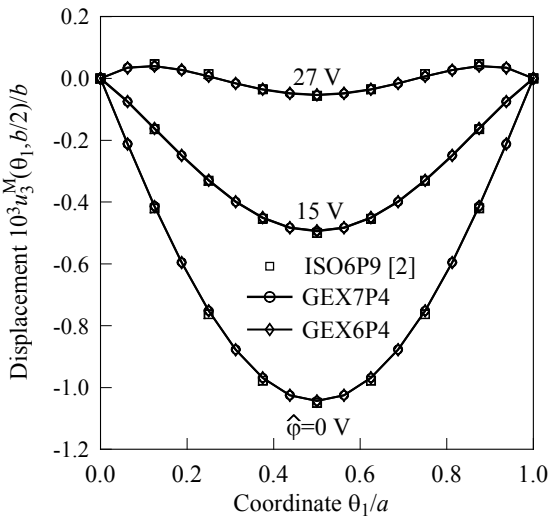

Figure 7. Midplane displacement of the simply supported plate.

The piezoceramic layers are polarized in opposite directions and subjected to a constant voltage of $\hat{\varphi} = 15\,\mathrm{V}$ and $27\,\mathrm{V}$. The electrodes on the interfaces are also assumed to be at the zero potential.

Due to symmetry of the problem, only one quarter of the plate is modeled by the uniform 8×8 mesh of GEX7P4 elements. Figure 7 shows the distribution of the transverse midplane displacement along the θ_1 - axis compared with numerical results [2, 4] derived by using identical node spacing. It is seen that all corresponding results are in a good agreement but the GEX finite element code is less expensive because no matrix inversions are needed and it is based on the 3D analytical integration.

7.4 Cantilever cylindrical shell with PZT actuators

Further, we investigate a response of the cantilever laminated cylindrical shell [15] made of above six graphite/epoxy layers with PZT G1195 actuators attached to the bottom and top surfaces and polarized in opposite directions parallel to the thickness direction. The geometrical and material properties of the shell are given in Figure 8 and Section 7.3. A ply orientation $[30/30/0]_S$ has been employed to induce the twisting actuation. Both piezoelectric layers are loaded statically at the outer surfaces by the electric potential of $\hat{\varphi} = 100\,\mathrm{V}$.

Figure 9 displays the tip displacement of the midsurface and the twist, defined as a difference between two end displacement values, versus a dimensionless radius of the curvature of its surface. The results have been derived with the 16×16 mesh of GEX7P4 elements and are compared with finite element solutions [2, 4] through using identical node spacing. As can be seen, both GEX solid-shell elements perform well again.

7.5 Cantilever hyperbolic shell with PVDF actuators

To demonstrate the high coarse-mesh accuracy of the GEX piezoelectric solid-shell element developed, we consider a six-layer graphite/epoxy hyperbolic shell covered with PVDF actuators on the bottom and top surfaces [4]. The material constants of PVDF are supposed to be $E = 2\,\mathrm{GPa}$, $\nu = 0.29$ and $d_{31} = d_{32} = 23\,\mathrm{pm/V}$, whereas the material constants of graphite/epoxy are represented in Section 7.3. A shell is assumed to be clamped on one of its edges as shown in Figure 10 and two stacking sequences $[0/90/0]_S$ and $[\gamma/\gamma/0]_S$ are studied, where γ is the angle between the asymptotic line and the tangent to the meridian. This angle is measured in the clockwise direction and may be evaluated by means of a simple formula [4]

$$\cos\gamma = \frac{A_1}{\sqrt{1+\mu}}, \qquad \mu = \frac{R^2 - r^2}{a^2}, \qquad A_1 = \sqrt{1 + \frac{\mu^2 z^2}{A_2^2}}, \qquad A_2 = r\sqrt{1 + \frac{\mu z^2}{r^2}}$$

The electric potential at outer surfaces of the piezoelectric layers is equal to the externally applied voltage of $1\,\mathrm{V}$ and at interfaces is treated as zero. Due to the opposite polarization of actuators, they will induce bending moments into the shell body and, therefore, in the case of the second ply sequence the twisting deformation will be generated.

A shell is discretized with regular meshes of GEX7P4 elements. Figure 11 shows the distribution of the midsurface displacement in the x-direction u_x^{M} along the z-axis and a comparison with results [4]. One can observe that the 6-parameter shell model overestimates again the tip displacement values. Additionally, Table 3 lists results of the convergence study. It should be noted that these results could not be easily achieved by the conventional isoparametric piezoelectric solid-shell elements with such coarse mesh configuration.

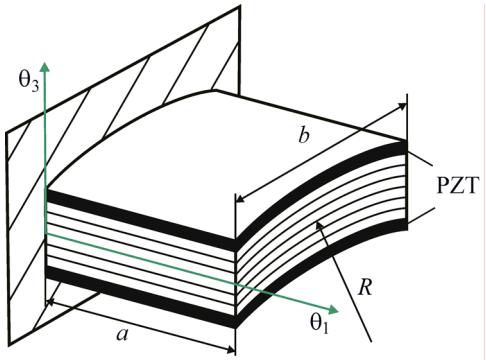

$a = b = 0.254\,\text{m}$, $h_{\text{PZT}} = 0.254\,\text{mm}$,
$h_{\text{C}} = 0.828\,\text{mm}$, $h = 1.336\,\text{mm}$

Figure 8: Cantilever cylindrical shell with PZT actuators.

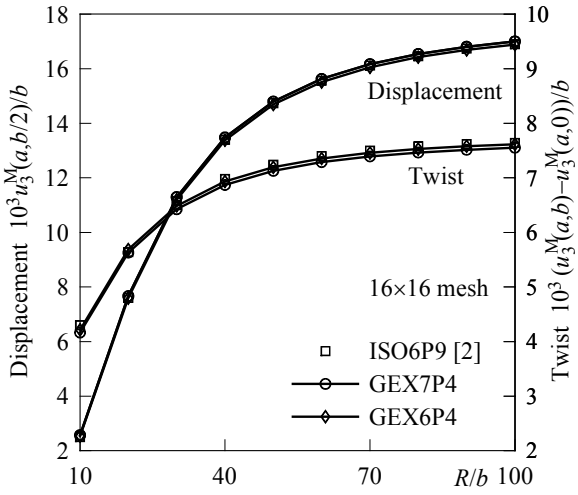

Figure 9: Tip midsurface displacements of the cantilever cylindrical shell.

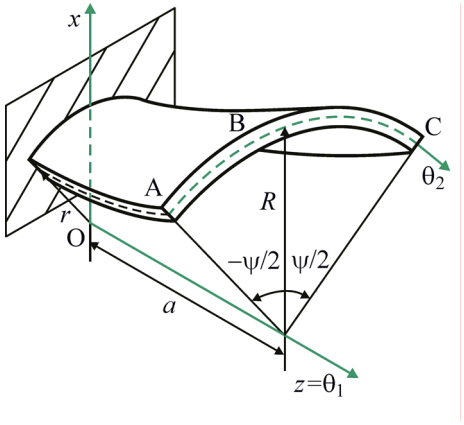

$a = 0.254\,\text{m}$, $r = 0.254\,\text{m}$, $R = 0.508\,\text{m}$, $h_{\text{PVDF}} = 0.254\,\text{mm}$,
$h_{\text{C}} = 0.828\,\text{mm}$, $h = 1.336\,\text{mm}$, $\psi = 20^{\circ}$

Figure 10: Cantilever hyperbolic shell with PVDF actuators.

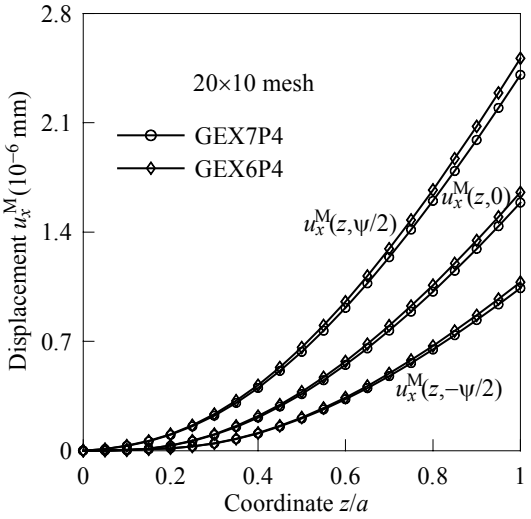

Figure 11: Midsurface displacements of the cantilever hyperbolic shell with ply orientation $[\gamma/\gamma/0]_{\text{S}}$.

	$[0/90/0]_{\text{S}}$				$[\gamma/\gamma/0]_{\text{S}}$			
Mesh	3×1	6×2	12×4	24×8	3×1	6×2	12×4	24×8
$-u_x^{\text{M}}(\text{A})$	0.5078	0.5877	0.5962	0.5958	1.093	0.943	1.020	1.042
$-u_x^{\text{M}}(\text{B})$		0.5311	0.5386	0.5382		1.479	1.563	1.590
$-u_x^{\text{M}}(\text{C})$	0.5078	0.5877	0.5962	0.5958	2.421	2.290	2.377	2.408

Table 3: Tip midsurface displacement $u_x^{\text{M}}\left(10^{-6}\,\text{m}\right)$ of the cantilever hyperbolic shell.

8 CONCLUSIONS

A new piezoelectric laminated solid-shell element model has been developed. In this model are utilized the objective strain-displacement relationships of the first-order 7-parameter ESL shell theory, which are invariant under all rigid-body shell motions. The simple and efficient hybrid stress-strain piezoelectric curved four-node solid-shell element is

based on the original approach in which displacement vectors of outer and middle surfaces are introduced but resolved, in contrast with the isoparametric solid-shell element formulation, in the reference surface frame. The GEX piezoelectric solid-shell element developed does not contain any spurious zero energy modes and its stiffness matrix possesses a correct rank. It is remarkable that all elemental matrices require only direct substitutions and they are evaluated by using the 3D analytical integration. So, our GEX piezoelectric solid-shell element is economical compared to conventional isoparametric finite elements because it additionally allows using very coarse meshes. Taking into account that electric signals generated by sensors are fed into microprocessors to activate a system of piezoelectric actuators in real time, a developed code is robust and very promising.

ACKNOWLEDGMENTS

The support of this work by Russian Ministry of Education and Science under Grant No 2.1.1/660 is gratefully acknowledged.

APPENDIX A

The mechanical, piezoelectric and dielectric constitutive matrices introduced in Section 5 are

$$\mathbf{D}_{\mathrm{M}} = \begin{bmatrix} D_{11}^{00} & D_{11}^{01} & D_{12}^{00} & D_{12}^{01} & D_{13}^{00} & D_{13}^{01} & D_{16}^{00} & D_{16}^{01} & 0 & 0 \\ & D_{11}^{11} & D_{12}^{01} & D_{12}^{11} & D_{13}^{01} & D_{13}^{11} & D_{16}^{01} & D_{16}^{11} & 0 & 0 \\ & & D_{22}^{00} & D_{22}^{01} & D_{23}^{00} & D_{23}^{01} & D_{26}^{00} & D_{26}^{01} & 0 & 0 \\ & & & D_{22}^{11} & D_{23}^{01} & D_{23}^{11} & D_{26}^{01} & D_{26}^{11} & 0 & 0 \\ & & & & D_{33}^{00} & D_{33}^{01} & D_{36}^{00} & D_{36}^{01} & 0 & 0 \\ & & & & & D_{33}^{11} & D_{36}^{01} & D_{36}^{11} & 0 & 0 \\ & & & & & & D_{66}^{00} & D_{66}^{01} & 0 & 0 \\ & & & & & & & D_{66}^{11} & 0 & 0 \\ & & & & & & & & D_{55} & D_{45} \\ \text{sym.} & & & & & & & & & D_{44} \end{bmatrix}$$

$$\mathbf{D}_{\mathrm{ME}}^{(\ell)} = \begin{bmatrix} -m_\ell^0 e_{31}^{(\ell)} & m_\ell^0 e_{31}^{(\ell)} & 0 & 0 & 0 & 0 \\ -m_\ell^1 e_{31}^{(\ell)} & m_\ell^1 e_{31}^{(\ell)} & 0 & 0 & 0 & 0 \\ -m_\ell^0 e_{32}^{(\ell)} & m_\ell^0 e_{32}^{(\ell)} & 0 & 0 & 0 & 0 \\ -m_\ell^1 e_{32}^{(\ell)} & m_\ell^1 e_{32}^{(\ell)} & 0 & 0 & 0 & 0 \\ -m_\ell^0 e_{33}^{(\ell)} & m_\ell^0 e_{33}^{(\ell)} & 0 & 0 & 0 & 0 \\ -m_\ell^1 e_{33}^{(\ell)} & m_\ell^1 e_{33}^{(\ell)} & 0 & 0 & 0 & 0 \\ -m_\ell^0 e_{36}^{(\ell)} & m_\ell^0 e_{36}^{(\ell)} & 0 & 0 & 0 & 0 \\ -m_\ell^1 e_{36}^{(\ell)} & m_\ell^1 e_{36}^{(\ell)} & 0 & 0 & 0 & 0 \\ 0 & 0 & k_\ell^0 e_{15}^{(\ell)} & k_\ell^1 e_{15}^{(\ell)} & k_\ell^0 e_{25}^{(\ell)} & k_\ell^1 e_{25}^{(\ell)} \\ 0 & 0 & k_\ell^0 e_{14}^{(\ell)} & k_\ell^1 e_{14}^{(\ell)} & k_\ell^0 e_{24}^{(\ell)} & k_\ell^1 e_{24}^{(\ell)} \end{bmatrix}$$

$$\mathbf{D}_{\mathrm{E}}^{(\ell)}=\begin{bmatrix} -h_\ell^{-1}\in_{33}^{(\ell)} & h_\ell^{-1}\in_{33}^{(\ell)} & 0 & 0 & 0 & 0 \\ & -h_\ell^{-1}\in_{33}^{(\ell)} & 0 & 0 & 0 & 0 \\ & & k_\ell^{00}\in_{11}^{(\ell)} & k_\ell^{01}\in_{11}^{(\ell)} & k_\ell^{00}\in_{12}^{(\ell)} & k_\ell^{01}\in_{12}^{(\ell)} \\ & & & k_\ell^{11}\in_{11}^{(\ell)} & k_\ell^{01}\in_{12}^{(\ell)} & k_\ell^{11}\in_{12}^{(\ell)} \\ & & & & k_\ell^{00}\in_{22}^{(\ell)} & k_\ell^{01}\in_{22}^{(\ell)} \\ \text{sym.} & & & & & k_\ell^{11}\in_{22}^{(\ell)} \end{bmatrix}$$

where

$$D_{ab}^{pq}=\sum_n m_n^{pq}C_{ab}^{(n)},\qquad D_{st}=\sum_n h_n C_{st}^{(n)}$$

$$m_n^{pq}=\int_{z_{n-1}}^{z_n}\left(N^-\right)^{2-p-q}\left(N^+\right)^{p+q}d\theta_3,\qquad m_\ell^{p}=\frac{1}{h_\ell}\int_{z_{\ell-1}}^{z_\ell}\left(N^-\right)^{1-p}\left(N^+\right)^{p}d\theta_3$$

$$k_\ell^{pq}=-\int_{z_{\ell-1}}^{z_\ell}\left(N_\ell^-\right)^{2-p-q}\left(N_\ell^+\right)^{p+q}d\theta_3,\qquad k_\ell^{p}=\int_{z_{\ell-1}}^{z_\ell}\left(N_\ell^-\right)^{1-p}\left(N_\ell^+\right)^{p}d\theta_3$$

where the indices introduced take the following values: $a,b=1,2,3,6$ and $s,t=4,5$, and $p,q=0,1$.

APPENDIX B

In order to fulfill the analytical integration throughout the element, we have to rewrite the strain approximation (29) as follows:

$$\boldsymbol{E}=\sum_{r_1,r_2}\xi_1^{r_1}\xi_2^{r_2}\boldsymbol{E}^{r_1r_2},\qquad \boldsymbol{E}^{r_1r_2}=\mathbf{B}_{\mathrm{M}}^{r_1r_2}\mathbf{U}$$
$$\boldsymbol{E}^{r_1r_2}=\left[\varepsilon_{11}^{-r_1r_2}\ \varepsilon_{11}^{+r_1r_2}\ \varepsilon_{22}^{-r_1r_2}\ \varepsilon_{22}^{+r_1r_2}\ \varepsilon_{33}^{-r_1r_2}\ \varepsilon_{33}^{+r_1r_2}\ 2\varepsilon_{12}^{-r_1r_2}\ 2\varepsilon_{12}^{+r_1r_2}\ 2\varepsilon_{13}^{\mathrm{M}r_1r_2}\ 2\varepsilon_{23}^{\mathrm{M}r_1r_2}\right]^{\mathrm{T}} \tag{B1}$$

Here, $\boldsymbol{E}^{r_1r_2}$ are the mode strain vectors, which are constant inside the element, and, as we remember, the superscripts r_1, r_2 run from 0 to 1. These vectors are evaluated using strain-displacement relationships (5)-(7) and bilinear approximation (B1):

$$\begin{aligned} 2\varepsilon_{\alpha\beta}^{Ar_1r_2}&=c_\alpha^{A00}\lambda_{\alpha\beta}^{Ar_1r_2}+c_\beta^{A00}\lambda_{\beta\alpha}^{Ar_1r_2},\qquad \varepsilon_{33}^{Ar_1r_2}=\beta_3^{Ar_1r_2} \\ 2\varepsilon_{\alpha3}^{\mathrm{M}r_1r_2}&=\varepsilon_{\alpha3}^{-r_1r_2}+\varepsilon_{\alpha3}^{+r_1r_2},\qquad 2\varepsilon_{\alpha3}^{Ar_1r_2}=c_\alpha^{A00}\beta_\alpha^{Ar_1r_2}+\lambda_{3\alpha}^{Ar_1r_2} \end{aligned} \tag{B2}$$

where

$$\begin{aligned} \lambda_{\alpha\alpha}^{Ar_1r_2}&=\left\{\frac{1}{A_\alpha^{\mathrm{el}}}u_\alpha^A\right\}_\alpha^{r_1r_2}+\left(B_{\alpha\alpha}u_\alpha^A+B_{\alpha\beta}u_\beta^A+k_\alpha u_3^A\right)^{r_1r_2}\ \text{ for }\ \beta\neq\alpha \\ \lambda_{\beta\alpha}^{Ar_1r_2}&=\left\{\frac{1}{A_\alpha^{\mathrm{el}}}u_\beta^A\right\}_\alpha^{r_1r_2}+\left(B_{\alpha\alpha}u_\beta^A-B_{\alpha\beta}u_\alpha^A\right)^{r_1r_2}\ \text{ for }\ \beta\neq\alpha \\ \lambda_{3\alpha}^{Ar_1r_2}&=\left\{\frac{1}{A_\alpha^{\mathrm{el}}}u_3^A\right\}_\alpha^{r_1r_2}+\left(B_{\alpha\alpha}u_3^A-k_\alpha u_\alpha^A\right)^{r_1r_2} \end{aligned} \tag{B3}$$

$$\beta_i^{-r_1r_2}=\frac{1}{h}\left(-3u_i^{-}+4u_i^{\mathrm{M}}-u_i^{+}\right)^{r_1r_2},\qquad \beta_i^{+r_1r_2}=\frac{1}{h}\left(u_i^{-}-4u_i^{\mathrm{M}}+3u_i^{+}\right)^{r_1r_2}$$

In equations (B2) and (B3) convenient mesh notations are employed (see Figure 2 with *NN*=4)

$$f^{00}=\frac{1}{4}\left[f(P_1)+f(P_2)+f(P_3)+f(P_4)\right],\qquad f^{10}=\frac{1}{4}\left[f(P_1)-f(P_2)-f(P_3)+f(P_4)\right]$$

$$f^{01}=\frac{1}{4}\left[f(P_1)+f(P_2)-f(P_3)-f(P_4)\right],\qquad f^{11}=\frac{1}{4}\left[f(P_1)-f(P_2)+f(P_3)-f(P_4)\right]$$

$$\{f\}_1^{00}=f^{10},\qquad \{f\}_1^{01}=f^{11},\qquad \{f\}_1^{10}=\{f\}_1^{11}=0$$

$$\{f\}_2^{00}=f^{01},\qquad \{f\}_2^{10}=f^{11},\qquad \{f\}_2^{01}=\{f\}_2^{11}=0$$

where $f(\xi_1,\,\xi_2)$ is any function; P_r are the nodal points of the element. Note also that derivatives from equations (7) are evaluated by means of a simple scheme as

$$\frac{\partial}{\partial\xi_1}\left(\frac{1}{A_1^{\mathrm{el}}}u_i^A\right)=\left(\frac{1}{A_1^{\mathrm{el}}}u_i^A\right)^{10}+\xi_2\left(\frac{1}{A_1^{\mathrm{el}}}u_i^A\right)^{11}$$

$$\frac{\partial}{\partial\xi_2}\left(\frac{1}{A_2^{\mathrm{el}}}u_i^A\right)=\left(\frac{1}{A_2^{\mathrm{el}}}u_i^A\right)^{01}+\xi_1\left(\frac{1}{A_2^{\mathrm{el}}}u_i^A\right)^{11}$$

Regarding a product $A_1^{\mathrm{el}}A_2^{\mathrm{el}}$ from formula (20), it does not vary inside the element and is evaluated at the center of the element as

$$A_1^{\mathrm{el}}A_2^{\mathrm{el}}=\left(A_1^{\mathrm{el}}A_2^{\mathrm{el}}\right)^{00}$$

This methodology plays a central role in derivation of the stiffness matrix with the help of the 3D analytical integration [9, 10] because allows us to calculate mode strain vectors $\boldsymbol{E}^{r_1r_2}$ through the node displacement values efficiently.

REFERENCES

[1] K.Y. Sze, L.Q. Yao and S. Yi, A hybrid stress ANS solid-shell element and its generalization for smart structure modelling. Part II – Smart structure modelling. *International Journal for Numerical Methods in Engineering*, **48**, 565–582, 2000.

[2] S. Lee, N.S. Goo, H.C. Park, K.J. Yoon and C. Cho, A nine-node assumed strain shell element for analysis of a coupled electro-mechanical system. *Smart Materials and Structures*, **12**, 355–362, 2003.

[3] S. Zheng, X. Wang and W. Chen, The formulation of a refined hybrid enhanced assumed strain solid shell element and its application to model smart structures containing distributed piezoelectric sensors/actuators. *Smart Materials and Structures*, **13**, N43-N50, 2004.

[4] G.M. Kulikov and S.V. Plotnikova, Geometrically exact four-node piezoelectric solid-shell element. *Mechanics of Advanced Materials and Structures*, **15**, 199–207, 2008.

[5] S.V. Plotnikova and M.G. Kulikov, Analysis of composite shells with piezoelectric patches. *Trans. Tambov State Technical University*, **15**, 380–391, 2009.

[6] G.M. Kulikov and S.V. Plotnikova, Simple and effective elements based upon Timoshenko-Mindlin shell theory. *Computer Methods in Applied Mechanics and Engineering*, **191**, 1173–1187, 2002.

[7] G.M. Kulikov and S.V. Plotnikova, Equivalent single-layer and layer-wise shell theories and rigid-body motions. Part I – Foundations, Part II – Computational aspects. *Mechanics of Advanced Materials and Structures*, **12**, 275–283, 331–340, 2005.

[8] H.S. Tzou, *Piezoelectric shells: Distributed sensing and control of continua*. Kluwer-Academic, Dordrecht, 1993.

[9] G.M. Kulikov and S.V. Plotnikova, Finite rotation geometrically exact four-node solid-shell element with seven displacement degrees of freedom. *Computer Modeling in Engineering & Sciences*, **28**, 15–38, 2008.

[10] G.M. Kulikov and S.V. Plotnikova, Geometrically exact assumed stress-strain multilayered solid-shell elements based on the 3D analytical integration. *Computers & Structures*, **84**, 1275–1287, 2006.

[11] G.M. Kulikov, Refined global approximation theory of multilayered plates and shells. *Journal of Engineering Mechanics*, **127**, 119–125, 2001.

[12] W.G. Cady, *Piezoelectricity: an introduction to the theory and applications of electromechanical phenomena in crystals.* Dover, New York, 1964.

[13] K.Y. Sze and L.Q. Yao, Modelling smart structures with segmented piezoelectric sensors and actuators. *Journal of Sound and Vibration*, **235**, 495–520, 2000.

[14] S.S. Vel and R.S. Batra, Analysis of piezoelectric bimorphs and plates with segmented actuators. *Thin-Walled Structures*, **39**, 23–44, 2001.

[15] H. Kioua and S. Mirza, Piezoelectric induced bending and twisting of laminated composite shallow shells. *Smart Materials and Structures*, **9**, 476–484, 2000.